Geophysical Research Letters

Supporting Information for

Magnitude and uncertainty in nitrous oxide emissions from North America based on bottom-up and top-down approaches

R. Xu[1,2], H. Tian[1], N. Pan[1], R. L. Thompson[3], J. G. Canadell[4], E. A. Davidson[5], C. Nevison[6], W. Winiwarter[7,8], H. Shi[1], S. Pan[1], J. Chang[9], P. Ciais[10], S. R. S. Dangal[11], A. Ito[12], R. B. Jackson[13], F. Joos[14], R. Lauerwald[15], S. Lienert[14], T. Maavara[16], D. B. Millet[17], P. A. Raymond[16], P. Regnier[18], F. N. Tubiello[19], N. Vuichard[10], K. C. Wells[17], C. Wilson[20,21], J. Yang[22], Y. Yao[1], S. Zaehle[23], F. Zhou[24]

[1]International Center for Climate and Global Change Research, School of Forestry and Wildlife Sciences, Auburn University, Auburn, AL, USA.

[2]Forest Ecosystems and Society, Oregon State University, Corvallis, OR, USA.

[3]Norsk Institutt for Luftforskning, NILU, Kjeller, Norway.

[4]Global Carbon Project, CSIRO Oceans and Atmosphere, Canberra, Australia.

[5]Appalachian Laboratory, University of Maryland Center for Environmental Science, Frostburg, MD, USA.

[6]University of Colorado Boulder/INSTAAR, Boulder, CO, USA.

[7]International Institute for Applied Systems Analysis, Laxenburg, Austria.

[8]Institute of Environmental Engineering, University of Zielona Góra, Zielona Góra, Poland.

[9]College of Environmental and Resource Sciences, Zhejiang University, Hangzhou, China.

[10]Laboratoire des Sciences du Climat et de l'Environnement, LSCE, CEA CNRS, UVSQ UPSACLAY, Gif sur Yvette, France.

[11]School of Natural Resources, University of Nebraska – Lincoln, NE, USA.

[12]Earth System Division, National Institute for Environmental Studies, Tsukuba, Japan.

[13]Department of Earth System Science, Woods Institute for the Environment, and Precourt Institute for Energy, Stanford University, Stanford, CA, USA.

[14]Climate and Environmental Physics, Physics Institute and Oeschger Centre for Climate Change Research, University of Bern, Bern, Switzerland.

[15]Université Paris-Saclay, INRAE, AgroParisTech, UMR ECOSYS, Thiverval-Grignon, France.

[16]Yale School of Forestry and Environmental Studies, New Haven, CT, USA.

[17]Department of Soil, Water, and Climate, University of Minnesota, MN, USA.

[18]Department Geoscience, Environment & Society-BGEOSYS, Université Libre de Bruxelles, Brussels, Belgium.

[19]Statistics Division, Food and Agriculture Organization of the United Nations, Via Terme di Caracalla, Rome, Italy.

[20]National Centre for Earth Observation, University of Leeds, Leeds, UK.

[21]Institute for Climate and Atmospheric Science, School of Earth and Environment, University of Leeds, Leeds, UK.

[22]Department of Forestry, Mississippi State University, Mississippi State, MS, USA.

[23]Max Planck Institute for Biogeochemistry, Jena, Germany.

[24]Sino-France Institute of Earth Systems Science, Laboratory for Earth Surface Processes, College of Urban and Environmental Sciences, Peking University, Beijing, China.

Corresponding author: Hanqin Tian (tianhan@auburn.edu)

Contents of this file

Figures S1 to S8
Tables S1 to S4

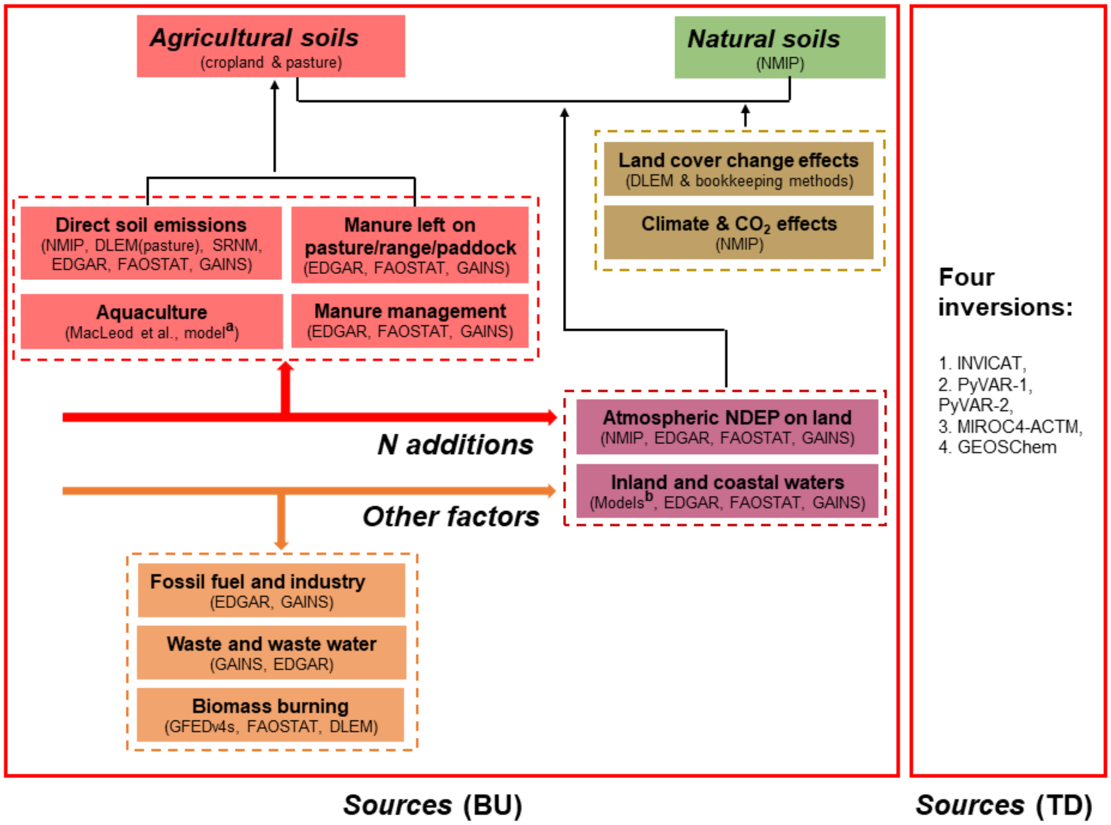

Figure S1. The methodology for data synthesis of North American N_2O sources. BU and TD represent bottom-up and top-down methods, respectively. The color codes are the same as that used in Table 1 and Figures. 1–2. We utilize both approaches, including 17 BU and five TD estimates of N_2O fluxes. For sources estimated by BU, we include six process-based terrestrial biosphere modeling studies (Tian et al., 2019); one nutrient budget model (Beusen et al., 2016; Bouwman et al., 2013; Bouwman et al., 2011); one inventory for aquaculture N_2O in 2013 (MacLeod et al., 2019); two inland water modeling studies (Lauerwald et al., 2019; Maavara et al., 2019; Yao et al., 2020); one statistical model SRNM based on spatial extrapolation of field measurements (Wang et al., 2019); and four GHG inventories: EDGAR v4.3.2 (Janssens-Maenhout et al., 2019), FAOSTAT (Tubiello et al., 2015), GAINS (Winiwarter et al., 2018), and GFED4s (Van Der Werf et al., 2017). [a]The nutrient budget model (Beusen et al., 2016; Bouwman et al., 2013; Bouwman et al., 2011) provides N flows in global freshwater and marine aquaculture over the period 1980–2016. [b]Model-based estimates of N_2O emissions from 'Inland and coastal waters' include rivers and reservoirs (Maavara et al., 2019; Yao et al., 2020), lakes (Lauerwald et al., 2019), and estuaries (Maavara et al., 2019).

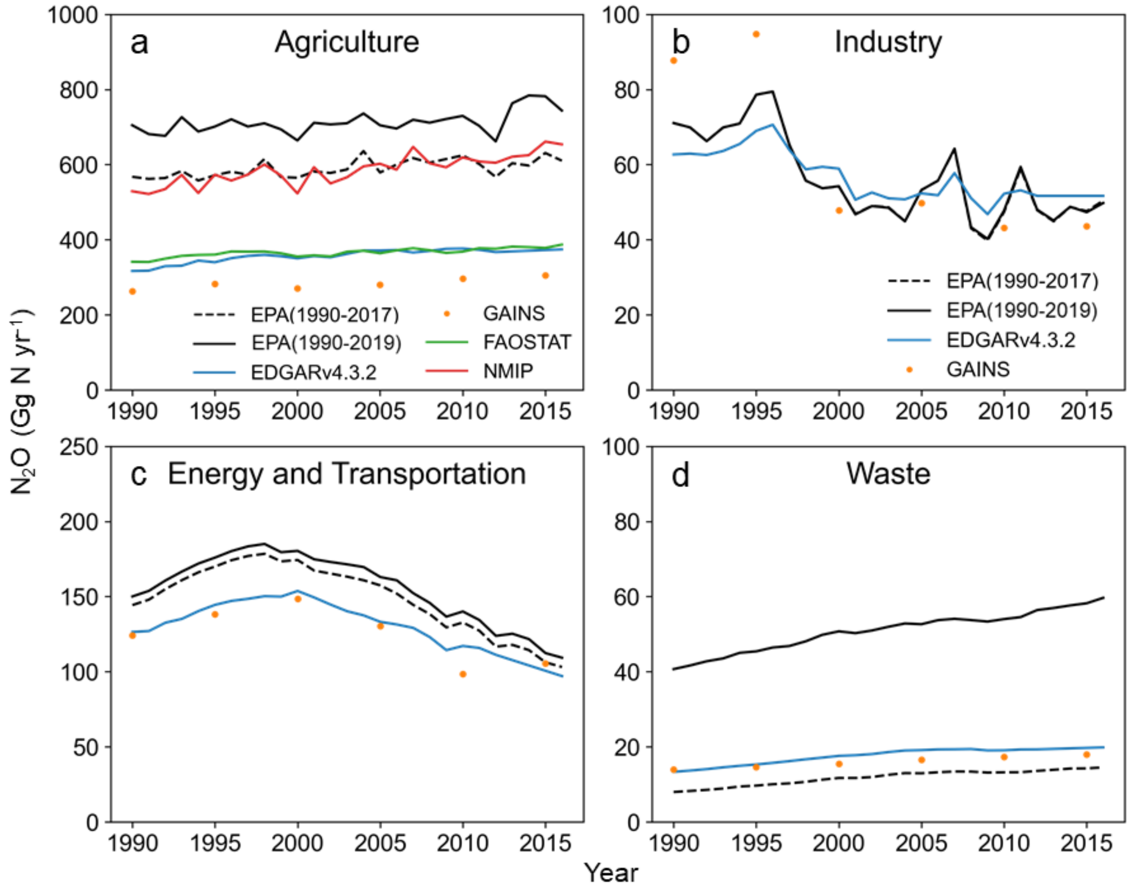

Figure S2. Comparison of our BU-estimated anthropogenic N_2O emissions with EPA during 1990–2016 in the U.S. Anthropogenic N_2O sectors include **(a)** agriculture, **(b)** industry, **(c)** energy and transportation, and **(d)** waste.

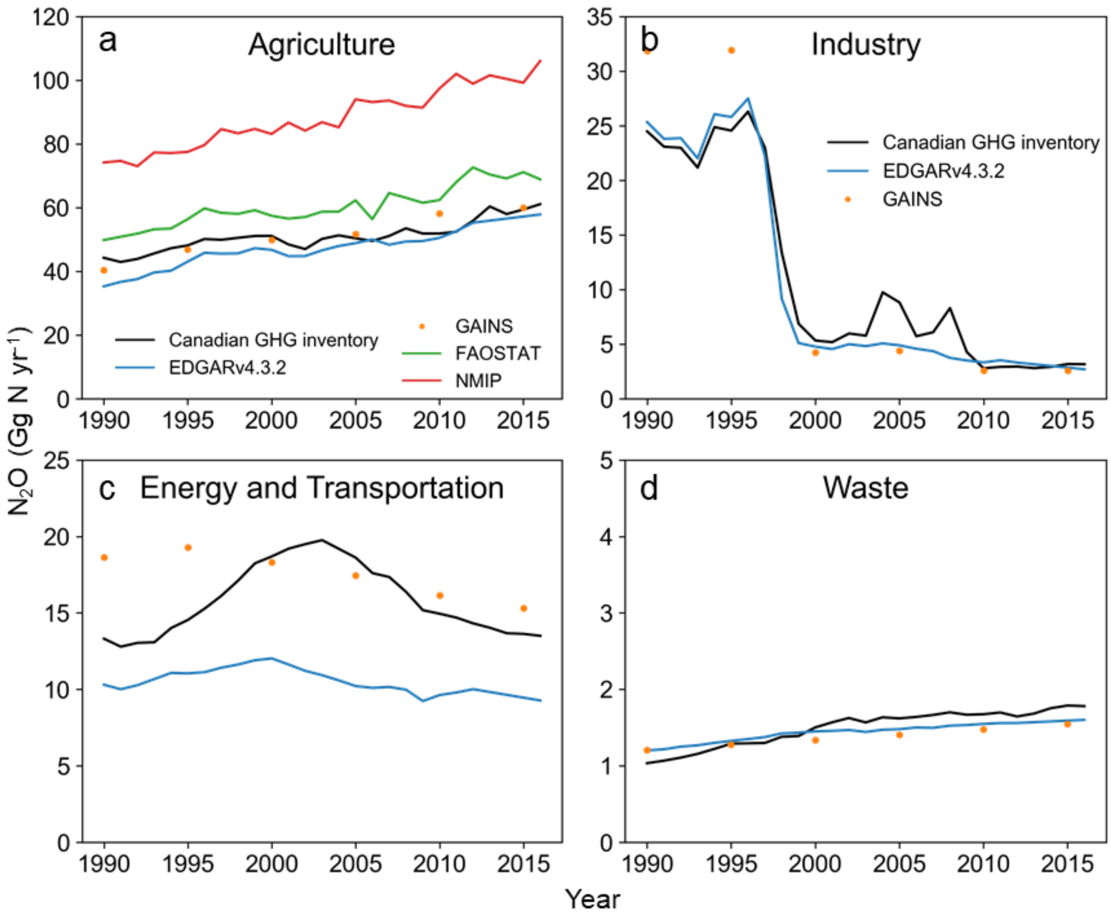

Figure S3. Comparison of our BU-estimated anthropogenic N_2O emissions with GHG inventory during 1990–2016 in Canada. Anthropogenic N_2O sectors include **(a)** agriculture, **(b)** industry, **(c)** energy and transportation, and **(d)** waste.

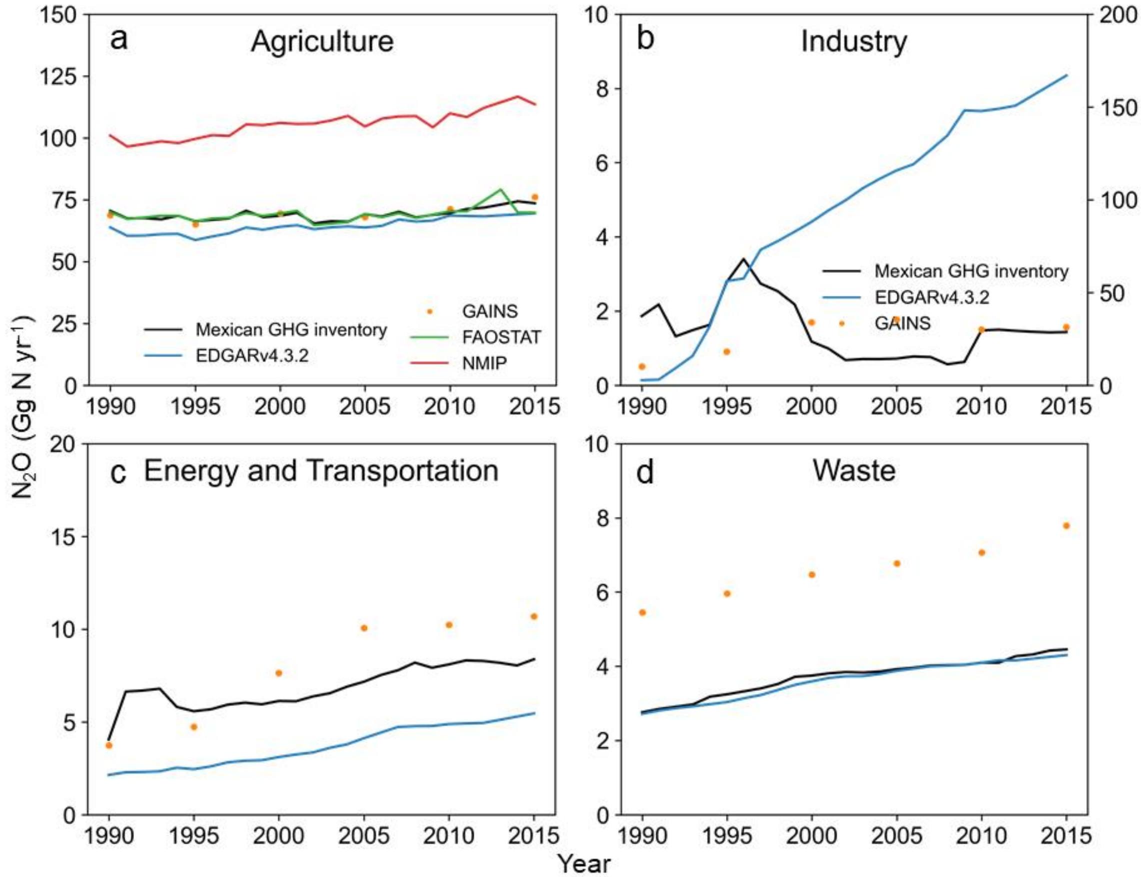

Figure S4. Comparison of our BU-estimated anthropogenic N_2O emissions with GHG inventory during 1990–2015 in Mexico. Anthropogenic N_2O sectors include **(a)** agriculture, **(b)** industry, **(c)** energy and transportation, and **(d)** waste.

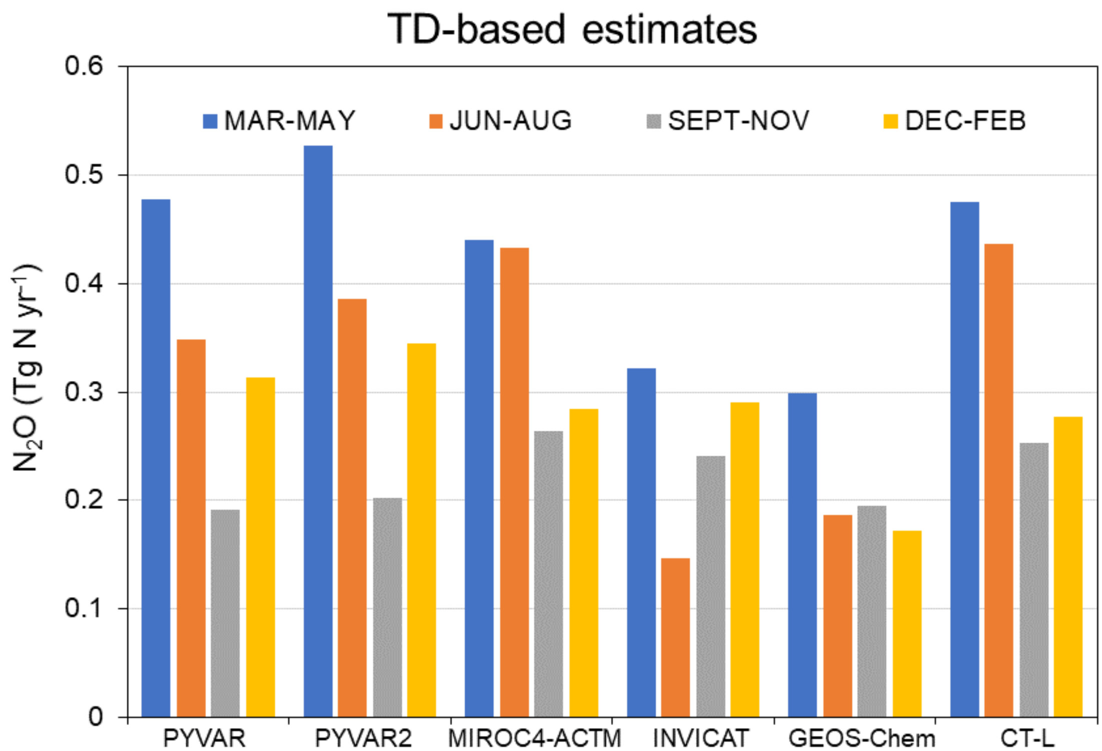

Figure S5. Seasonal total N_2O fluxes from TD approaches over North America between 2008 and 2013. Five TD inversion models include PYVAR-CAMS, MIRCO4-ACTM, INVICAT, GEOS-Chem, and CT-L.

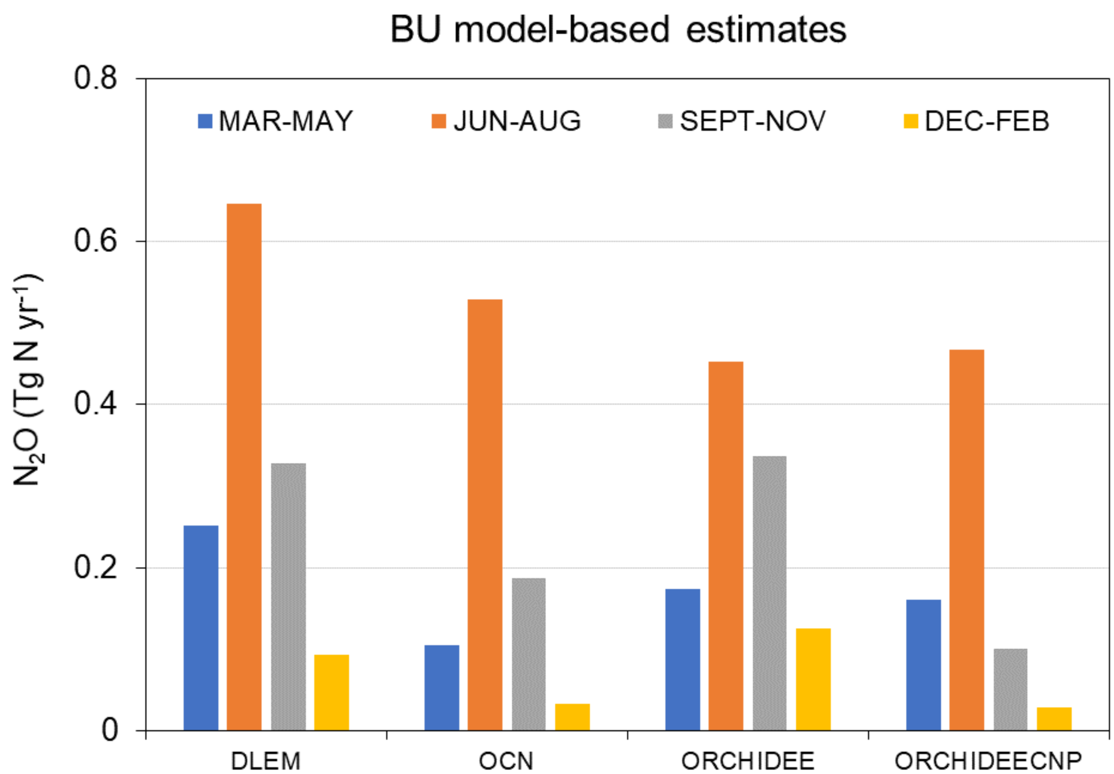

Figure S6. Seasonal cropland N_2O fluxes from BU approaches over North America between 2007 and 2016. Four terrestrial biosphere models include DLEM, OCN, ORCHIDEE, and ORCHIDEE-CNP.

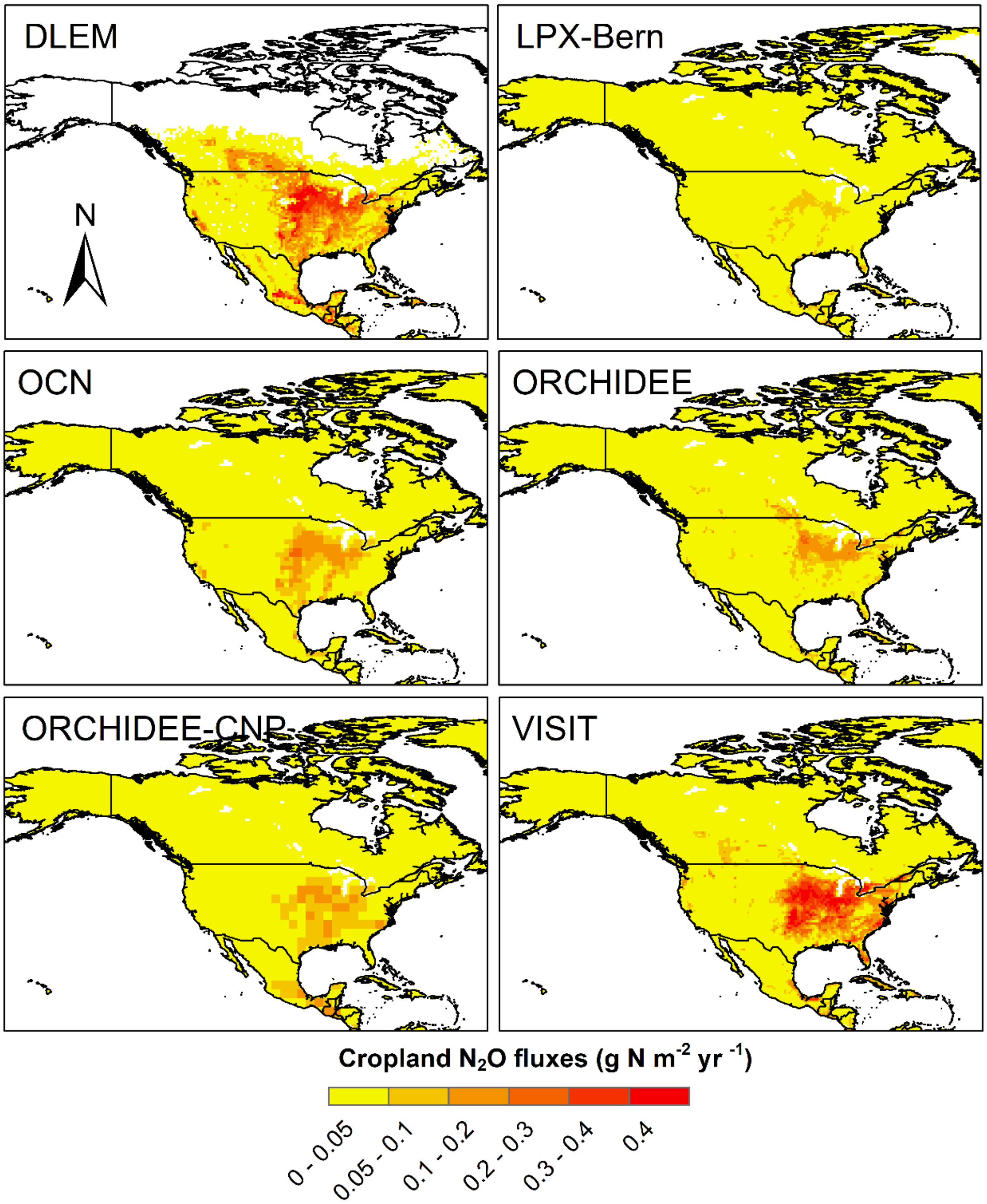

Figure S7. Spatial distribution of cropland N_2O emissions by BU approaches. Six terrestrial biosphere models include DLEM, LPX-Bern, OCN, ORCHIDEE, ORCHIDEE-CNP, and VISIT.

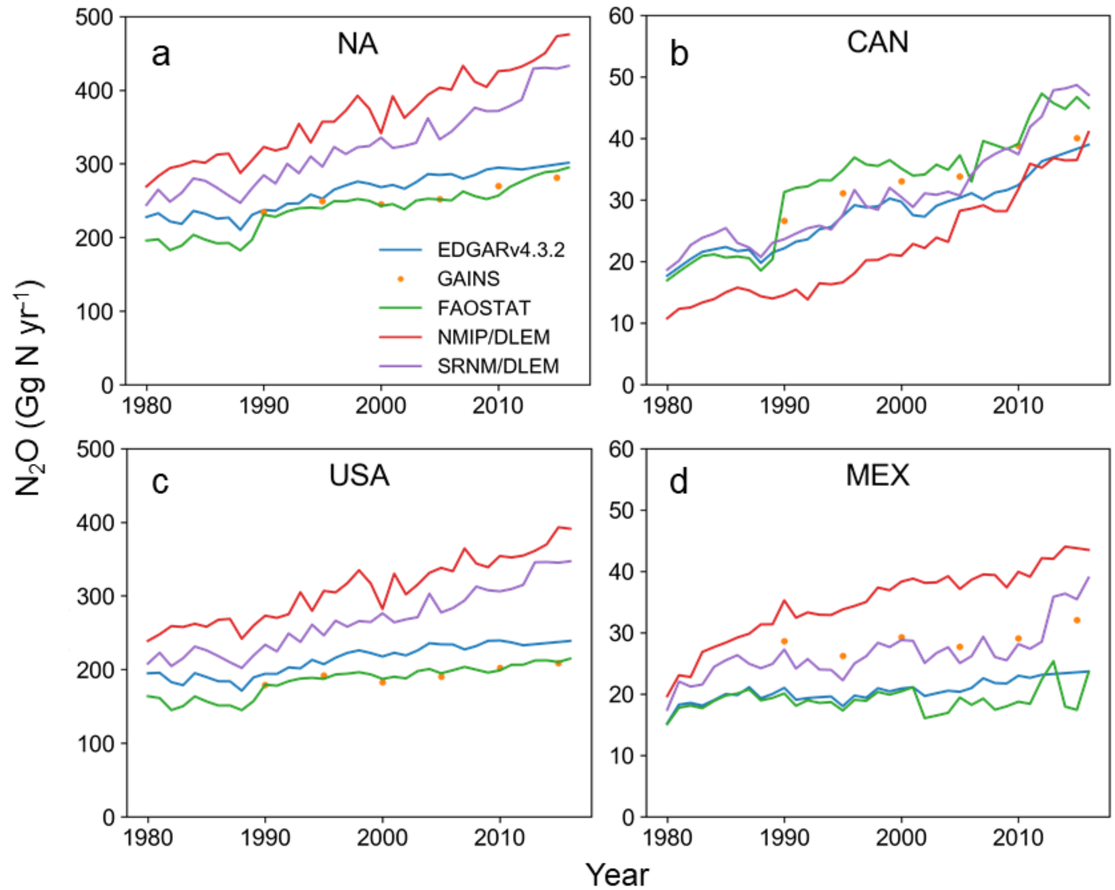

Figure S8. Direct emission from agricultural soils associated with mineral fertilizer, manure and crop residue inputs, and cultivation of organic soils based on EDGAR v4.3.2, GAINS, FAOSTAT, NMIP/DLEM, and SRNM/DLEM estimates in **(a)** North America, **(b)** Canada, **(c)** the U.S., and **(d)** Mexico.

Table S1. Decadal changes in anthropogenic N_2O sources over the past four decades over North America including the U.S., Canada, and Mexico.

		Decadal change (%)			
Anthropogenic sources		USA	Canada	Mexico	North America
Direct emissions of N additions in the agricultural sector (Agriculture)	Direct soil emissions	41	101	33	45
	Manure left on pasture	-7	30	7	-6
	Manure management	1	31	5	17
	Aquaculture	N/A	N/A	N/A	124
	sub-total	**27**	**80**	**18**	**29**
Other direct anthropogenic sources	Fossil fuel and industry	-26	-61	2283	1
	Waste and waste water	45	34	57	47
	Biomass burning				
	sub-total	**-22**	**-58**	**1168**	**3**
Indirect emissions from anthropoenic N additions	Inland waters, estuaries, coastal zones	12	10	1	10
	Atmospheric N deposition on land	-2	19	33	4
	sub-total	**3**	**13**	**20**	**6**
Perturbed fluxes from climate/CO2/land cover change	Climate & CO_2 effect	73	61	112	66
	Post-deforestation pulse effect	-3	-12	-14	-5
	Long-term effect of reduced mature forest area	-7	-1	19	0
	sub-total	**18**	**11**	**137**	**9**
Anthropogenic total		**7**	**-1**	**114**	**14**

Table S2. Information on North American N_2O measurement sites used in the global inversions from 1995 to 2016. CCG represents for discrete air samples from the National Oceanic and Atmospheric Administration Carbon Cycle Cooperative Global Air Sampling Network (NOAA); CSI represents for N2O measurements from the Commonwealth Scientific and Industrial Research Organization network (CSIRO); and AGA and CAT represent for N2O measurements from in-situ instruments in the Advanced Global Atmospheric Gases Experiment network (AGAGE) and the NOAA CATS network, respectively.

The global inversions: PyVAR-CAMS, INVICAT, GEOS-Chem				
Sites	**Latitude (°)**	**Longitude (°)**	**Altitude (m)**	**Type (FM: flask; CM: continuous)**
ALT_CCG	82.45	-62.52	205	FM
ALT_CSI	82.45	-62.52	210	FM
BAO_CCG	40.05	-105.01	1884	FM
BRW_CAT	71.32	-156.61	11	CM
BRW_CCG	71.32	-156.61	13	FM
CBA_CCG	55.21	-162.72	25	FM
ESP_CSI	49.38	-126.55	39	FM
HSU_CCG	41.05	-124.73	7.6	FM
KEY_CCG	25.67	-80.2	6	FM
KUM_CCG	19.52	-154.82	8	FM
LEF_CCG	45.93	-90.27	868	FM
LLB_CCG	54.95	-112.45	546	FM
MEX_CCG	18.98	-97.31	4469	FM
MID_CCG	28.22	-177.37	11	FM
MLO_CAT	19.54	-155.58	3397	CM
MLO_CCG	19.53	-155.58	3402	FM
MLO_CSI	19.53	-155.58	3397	FM
MVY_CCG	41.33	-70.51	12	FM
MWO_CCG	34.22	-118.06	1774	FM
NWR_CAT	40.05	-105.58	3526	CM
NWR_CCG	40.05	-105.58	3526	FM
PTA_CCG	38.95	-123.73	22	FM
SCT_CCG	33.41	-81.83	420	FM
SGP_CCG	36.62	-97.48	374	FM
SHM_CCG	52.72	174.1	28	FM
STR_CCG	37.75	-122.45	370	FM
THD_AGA	41.05	-124.15	107	CM
THD_CCG	41.05	-124.15	112	FM
UTA_CCG	39.9	-113.72	1332	FM
WBI_CCG	41.72	-91.35	621	FM
WGC_CCG	38.26	-121.49	483	FM
The global inversion: MIROC4-ACTM				
Sites	**Latitude (°)**	**Longitude (°)**	**Altitude (m)**	**Type (FM: flask)**
BRW_CCG	71.32	-156.61	11	FM
CBA_CCG	55.21	-162.72	21.34	FM
KUM_CCG	19.52	-154.82	3	FM
KEY_CCG	25.67	-80.16	1	FM
NWR_CCG	40.05	-105.59	3523	FM

Table S3. Information on North American N_2O measurement sites used in the CT-L regional inversion from 2007 to 2015 (Modified from Nevison et al., 2018).

Site	Latitude (°)	Longitude (°)	Altitude m agl (*asl)	Number of Measurements	Data Period
Surface Sites					
AMT	45.0	-68.7	107	1460	1/07-12/15
BAO	40.1	-105.0	300	2880	8/07-12/15
BMW	32.3	-64.9	30	341	1/07-12/15
BRW	71.3	-156.6	17	933	1/07-12/15
CBA	55.2	-162.7	36	656	1/07-12/15
CRV	65.0	-147.6	32	824	10/11-12/15
HSU	41.0	-124.3	8	72	5/08-12/15
INX	39.6 to 39.9	-86.4 to -85.7	156 to 225	1168	10/10-12/15
KEY	25.7	-80.2	5	394	1/07-12/15
LEF	45.9	-90.3	244 or 396	3138	1/07-12/15
LLB	55.0	-112.5	48	193	1/08-2/13
MBO	44.0	-121.7	11	629	10/11-5/14
MEX	19.0	-97.3	4469*	282	1/09-12/15
MLS	39.5 to 40.6	-110.2 to -104.5	0 to 13	289	6/08-7/08 and 6/11-6/12
MWO	34.2	-118.1	1774*	2040	4/10-12/15
NWR	40.0	-105.6	3526*	730	1/07-12/15
POC	10 to 35	-145 to -118	20	258	1/07-1/12
SCT	33.4	-81.8	305	1867	8/08-12/15
SGP	36.6	-97.5	60	452	1/07-12/15
STR	37.8	-122.5	486*	4036	10/07-12/15
THD	41.0	-124.2	5	453	1/07-12/15
UTA	39.9	-113.7	5	333	1/07-12/15
WBI	41.7	-91.4	379	2876	6/07-12/15
WGC	38.3 to 39.3	-121.5	91	2037	9/07-12/15
WKT	31.3	-97.3	5, 122 or 457	2427	1/07-12/15
Aircraft Sites					
ACG	57.0 to 76.6	-169.7 to -131.8	883 to 7969	1382	6/09-9/15
CAR	40.1 to 40.9	-105.2 to -104.1	665 to 6658	2246	1/07-12/15
CMA	38.4 to 39.0	-76.5 to -74.1	284 to 7422	1858	1/07-12/15
DND	47.2 to 48.5	-99.5 to -96.2	138 to 7002	1202	1/07-12/15
ESP	49.3 to 49.6	-126.6 to -125.7	314 to 5149	2432	1/07-12/15
ETL	53.9 to 54.6	-105.3 to -104.4	463 to 6165	2180	1/07-12/15
HIL	39.9 to 40.2	-88.1 to -87.7	727 to 7549	1642	1/07-12/15
LEF	45.7 to 46.1	-90.4 to -89.9	160 to 3250	2133	1/07-12/15
MLS	32.1 to 48.8	-112.2 to -96.1	2 to 3390	760	2/12-10/15
NHA	42.8 to 43.1	-70.7 to -70.3	321 to 7300	2241	1/07-12/15
PFA	64.1 to 65.9	-151.1 to -146.0	2343 to 6467	2342	1/07-12/15
SCA	32.5 to 33/9	-79.8 to -79.3	332 to 7861	1888	1/07-12/15
THD	40.9 to 41.6	-124.4 to -123.9	311 to 7901	1236	1/07-12/15
TGC	27.4 to 27.9	-97.0 to -96.5	317 to 7893	1434	1/07-12/15
WBI	41.6 to 42.5	-91.9 to -91.1	372 to 6372	1376	1/07-12/15

Table S4. Overview of the global and regional inversion frameworks.

	Name	Method	ACTM horizontal resolution	Ocean prior
Global inversion models	INVICAT	4D-Var	5.625°×5.625°	1 (high)
	PyVAR-CAMS-1	4D-Var	3.75°×1.875°	1 (high)
	PyVAR-CAMS-2			2 (low)
	MIROC4-ACTM	Bayesian analytical	2.8°×2.8°	3 (low)
	GEOS-Chem	4D-Var	5°×4°	2 (low)
Regional inversion model	CT-L	Bayesian analytical	1°×1°	NA

References

Beusen, A. H., Bouwman, A. F., Van Beek, L. P., Mogollón, J. M., & Middelburg, J. J. (2016). Global riverine N and P transport to ocean increased during the 20th century despite increased retention along the aquatic continuum. *Biogeosciences, 13*(8), 2441-2451.

Bouwman, A. F., Beusen, A., Overbeek, C., Bureau, D., Pawlowski, M., & Glibert, P. (2013). Hindcasts and future projections of global inland and coastal nitrogen and phosphorus loads due to finfish aquaculture. *Reviews in Fisheries Science, 21*(2), 112-156.

Bouwman, A. F., Pawłowski, M., Liu, C., Beusen, A. H., Shumway, S. E., Glibert, P., & Overbeek, C. (2011). Global hindcasts and future projections of coastal nitrogen and phosphorus loads due to shellfish and seaweed aquaculture. *Reviews in Fisheries Science, 19*(4), 331-357.

FAO, 2021. FAOSTAT Emissions database, http://www.fao.org/faostat/en/#data/GT, FAO, Rome, Italy.

Janssens-Maenhout, G., Crippa, M., Guizzardi, D., Muntean, M., Schaaf, E., Dentener, F., et al. (2019). EDGAR v4.3.2 Global Atlas of the three major greenhouse gas emissions for the period 1970–2012. *Earth System Science Data, 11*(3), 959-1002. https://www.earth-syst-sci-data.net/11/959/2019/

Lauerwald, R., Regnier, P., Figueiredo, V., Enrich-Prast, A., Bastviken, D., Lehner, B., et al. (2019). Natural lakes are a minor global source of N_2O to the atmosphere. *Global Biogeochemical Cycles, 33*, 1564-1581.

Maavara, T., Lauerwald, R., Laruelle, G. G., Akbarzadeh, Z., Bouskill, N. J., Van Cappellen, P., & Regnier, P. (2019). Nitrous oxide emissions from inland waters: Are IPCC estimates too high? *Global change biology, 25*(2), 473-488.

MacLeod, M., Hasan, M. R., Robb, D. H. F., & Mamun-Ur-Rashid, M. (2019). *Quantifying and mitigating greenhouse gas emissions from global aquaculture*. Retrieved from Rome.

Nevison, C., Andrews, A., Thoning, K., Dlugokencky, E., Sweeney, C., Miller, S., et al. (2018). Nitrous Oxide Emissions Estimated With the CarbonTracker-Lagrange North American Regional Inversion Framework. *Global Biogeochemical Cycles, 32*(3), 463-485.

Tian, H. Q., Yang, J., Xu, R. T., Lu, C. Q., Canadell, J. G., Davidson, E. A., et al. (2019). Global soil nitrous oxide emissions since the preindustrial era estimated by an ensemble of terrestrial biosphere models: Magnitude, attribution, and uncertainty. *Global change biology, 25*(2), 640-659. <Go to ISI>://WOS:000456028900021

Tubiello, F., Cóndor-Golec, R., Salvatore, M., Piersante, A., Federici, S., Ferrara, A., et al. (2015). *Estimating greenhouse gas emissions in agriculture: a manual to address data requirements for developing countries*. Retrieved from Rome

Van Der Werf, G. R., Randerson, J. T., Giglio, L., Van Leeuwen, T. T., Chen, Y., Rogers, B. M., et al. (2017). Global fire emissions estimates during 1997-2016. *Earth System Science Data, 9*, 697-720.

Wang, Q., Zhou, F., Shang, Z., Ciais, P., Winiwarter, W., Jackson, R. B., et al. (2019). Data-driven estimates of global nitrous oxide emissions from croplands. *National Science Review, 00*, 1-12.

Winiwarter, W., Höglund-Isaksson, L., Klimont, Z., Schöpp, W., & Amann, M. (2018). Technical opportunities to reduce global anthropogenic emissions of nitrous oxide. *Environmental Research Letters, 13*(1), 014011.

Yao, Y., Tian, H., Shi, H., Pan, S., Xu, R., Pan, N., & Canadell, J. G. (2020). Increased global nitrous oxide emissions from streams and rivers in the Anthropocene. *Natural Climate Change, 10*(2), 138-142.

180